

Influence of Cobalt Doping on the Physical Properties of $\text{Zn}_{0.9}\text{Cd}_{0.1}\text{S}$ Nanoparticles

Sonal Singhal · Amit Kumar Chawla ·
Hari Om Gupta · Ramesh Chandra

Received: 10 September 2009 / Accepted: 28 October 2009 / Published online: 17 November 2009
© to the authors 2009

Abstract $\text{Zn}_{0.9}\text{Cd}_{0.1}\text{S}$ nanoparticles doped with 0.005–0.24 M cobalt have been prepared by co-precipitation technique in ice bath at 280 K. For the cobalt concentration >0.18 M, XRD pattern shows unidentified phases along with $\text{Zn}_{0.9}\text{Cd}_{0.1}\text{S}$ sphalerite phase. For low cobalt concentration (≤ 0.05 M) particle size, d_{XRD} is ~ 3.5 nm, while for high cobalt concentration (>0.05 M) particle size decreases abruptly (~ 2 nm) as detected by XRD. However, TEM analysis shows the similar particle size (~ 3.5 nm) irrespective of the cobalt concentration. Local strain in the alloyed nanoparticles with cobalt concentration of 0.18 M increases $\sim 46\%$ in comparison to that of 0.05 M. Direct to indirect energy band-gap transition is obtained when cobalt concentration goes beyond 0.05 M. A red shift in energy band gap is also observed for both the cases. Nanoparticles with low cobalt concentrations were found to have paramagnetic nature with no antiferromagnetic coupling. A negative Curie–Weiss temperature of -75 K with antiferromagnetic coupling was obtained for the high cobalt concentration.

Keywords Cobalt doping · Paramagnetism · Quantum confinement

Introduction

Semiconductor nanoparticles have generated great fundamental and technical interests due to novel size-tunable properties and, consequently, in potential applications as optoelectronic devices and biomedical tags [1–5]. In the last two decades, the main efforts have been focused on the preparation of different colour-emitting binary or core-shell nanoparticles with different particle sizes [6–9]. However, the tuning of physical and chemical properties by changing the particle size could cause problems in many applications, in particular, if unstable small particles (less than 2 nm) are used [10]. Recent advances have led to the exploration of tunable optical properties by changing their constituent stoichiometries in mixed ternary nanoparticles [11]. The introduction of transition metal (TM) into non-magnetic semiconductors provide another possible way for generation of diluted magnetic semiconductors (DMS) [3, 12]. DMS can play a vital role in the field of spintronics because of its ability to accommodate electron charge and its spin degrees of freedom into single matter and their interplay can explore new functionality [13]. There are contradictory reports on magnetic behaviour of these materials such as many people have reported presence of ferromagnetism in DMS systems, whereas some reported its absence [12–15]. Continuous attempts are being made to synthesize sulphide nanomaterials with controlled sizes, shapes, and phase purity by various chemical routes [16–18]. The advantages of chemical routes over other synthesis methods are: (a) easier control of the oxidation states, (b) ability to make nanostructures of different sizes and shapes, (c) relatively cheap. Wang et al. [7] reported the one-dimensional nanocomposites of CdS/ZnS . Mehta et al. [18] synthesized the ZnS nanoparticles via facile CTAB aqueous micellar solution rout. It has been found

S. Singhal · A. K. Chawla · R. Chandra (✉)
Nanoscience Laboratory, Institute Instrumentation Center,
Indian Institute of Technology Roorkee, Roorkee 247667, India
e-mail: ramesfic@iitr.ernet.in; ramesfic@gmail.com

S. Singhal · H. O. Gupta
Department of Electrical Engineering, Indian Institute
of Technology Roorkee, Roorkee 247667, India

that nanocrystals with dopants inside their crystal lattice can exhibit different properties from those with ones on their surface [19]. However, experimental data is still lacking on the fundamental question of whether different dopant positions inside nanocrystals can affect physical properties of doped nanocrystals. Homogeneously substitutional doping is one of the most important goals for achieving novel physical properties in TM-doped nano-sized semiconductors [20, 21].

In nanoparticles the systematic tuning of their band gap can be controlled by alloy formation as well as by size variation. Sung et al. and Yang et al. demonstrated that for undoped ternary nanoparticles, energy band gap can be tuned as a function of their composition including $Zn_{1-x}Cd_xSe$ [22–24] and $CdSe_{1-x}Te_x$ [25]. As an II–VI semiconductor, $Zn_{1-x}Cd_xS$ is considered to be a promising host material. Zhong et al. [26] and Bhargava et al. [27] studies reveal that Mn-doped ZnS nanoparticles show significant increase in luminescence intensity and is due to the strong interaction of d electrons of Mn^{2+} with s–p electrons of the host nanocrystalline Zn. Zielinski et al. [28] and Seong et al. [29] reported that the sp–d exchange interactions in Co^{2+} -doped II–VI semiconductors are much larger than those in the Mn^{2+} -doped counterparts. In this study, cobalt-doped $Zn_{0.9}Cd_{0.1}S$ alloyed ($Zn_{0.9}Cd_{0.1}S:yCo$) nanoparticles with different cobalt doping concentrations were prepared by the co-precipitation method. With the aid of structural, magnetic and quantitative analyses, we demonstrated that the dopants are embedded within the nanoparticles. The relationship of physical properties of $Zn_{0.9}Cd_{0.1}S:yCo$ nanoparticles to the doping amount is explored systematically.

Experimental

Cobalt-doped $Zn_{0.9}Cd_{0.1}S$ alloyed nanoparticles were synthesized using the co-precipitation method without capping ligand or surfactant. Requisite amounts of 0.5 M zinc nitrate, 0.05 M cadmium nitrate and appropriate molar amount of cobalt nitrate aqueous solution were mixed thoroughly. 0.5 M sodium sulphide aqueous solution was added into the above mixture drop by drop along with continuous stirring at 280 K in ice bath. The particles were then centrifuged, rinsed with distilled water and dried in a hot air oven at 320 K. A series of $Zn_{0.9}Cd_{0.1}S$ alloyed nanoparticles doped with cobalt concentrations of 0.0, 0.005, 0.01, 0.015, 0.025, 0.05, 0.12, 0.18 and 0.24 M were prepared. Doping concentrations of cobalt were determined by Electron Probe Micro Analyzer (Cameca SX 100). The particle size, shape and orientations of the nanoparticles were determined by transmission electron microscope (FEI TECNAI-G²). X-ray analysis was performed using a

Bruker D8 Advance diffractometer with Cu K $_{\alpha}$ target ($\lambda = 1.54056 \text{ \AA}$) radiation. Optical absorption was measured in the 200–800 nm wavelength range using UV–Vis–NIR spectrophotometer (Varian Cary 5000). Magnetic measurements were taken with superconducting quantum interference device (SQUID) magnetometer (QD MPMS-XL).

Results and Discussions

Determination of phase composition, structure and particle size are very important for the discussions on the physical properties. EPMA analysis determines the cobalt concentration in the doped nanoparticles. Obtained cobalt values (y) in molar amount are found lower than the cobalt concentrations in the starting solution for all the samples and are shown in Table 1. Figure 1 shows the XRD patterns of the $Zn_{0.9}Cd_{0.1}S:yCo$ alloyed nanoparticles. Broad diffraction peaks in all the patterns were in agreement with the characteristics of nanosized materials. It can be seen that the nanoparticles with cobalt concentration (≤ 0.18 M) exhibited a sphalerite structure with (111), (220) and (311) orientations, which was consistent with the result that ZnS exist in sphalerite structure at low temperature [27, 30]. However, the (111) diffraction peak of undoped sample i.e., $Zn_{0.9}Cd_{0.1}S$ shifted to a lower angle from 28.6° to 28.45° from the standard Sphalerite structure of ZnS [31]. This shift towards lower angle is believed to result from the incorporation of Cd ions into the ZnS lattice, and the larger ionic radius of Cd^{2+} as compared to that of Zn^{2+} (Cd^{2+} : 0.97 \AA , Zn^{2+} : 0.74 \AA). Crystallite size was estimated from the full width at half maximum of the major XRD peak using the Scherrer equation [32]. Here, we found that for $Zn_{0.9}Cd_{0.1}S:yCo$ samples the calculated average size is ~ 3.5 nm when the cobalt concentration in nanoparticles is less than or equal to 0.05 M. For the sample with cobalt concentration of 0.18 M, the average particle size decreases abruptly to ~ 2 nm. Cobalt concentration greater than 0.18 M produces a greater amount of distortion in the lattice and the XRD pattern shows unidentified phases along with $Zn_{0.9}Cd_{0.1}S$ sphalerite phase. In order to find out the extent of strain that have been induced in the lattice due to cobalt incorporation, strain analysis has also been carried out. Local strain is calculated by making use of Scherrer formula of Δk versus k (the scattering vector $k = (4\pi/\lambda)\sin\theta$) [33]. The three peaks of (111), (220) and (311) were fitted linearly to obtain the local strain values. Calculated values of local strain are shown in Table 1. On the left axis of Fig. 2, local strain values are shown with variation in molar cobalt concentration. It can be seen that the crystallinity of doped nanoparticles (see Fig. 1) is fairly good as the local strain values are smaller when the cobalt

concentration in the nanoparticles is less than 0.12 M. Increasing cobalt concentration up to 0.18 M caused the abrupt rise in local strain values, giving rise to large distortion in the lattice and thus degrades the crystallinity. At cobalt concentration of 0.24 M, it was not possible to calculate the strain values, as the XRD spectra shows the unidentified orientation along with the (111), (220) and (311) orientations. It can also be observed from Fig. 1 that there is a slight shift in the XRD peak position towards higher angles with increase in cobalt concentration, resulting in change in the lattice constant. On the right axis of Fig. 2, lattice constant of Zn_{0.9}Cd_{0.1}S: yCo nanoparticles for different cobalt concentrations are shown. Lattice constants decrease with increase in the cobalt concentration. Singh et al. [14] have reported the similar dependence of the lattice constant on cobalt doping in ZnO matrix. Moreover, this also reflects that Co²⁺ ions were substituted without changing the sphalerite structure. This is quite expected as the ionic radii of the Co²⁺ in the tetrahedral coordination are nearly the same as that of zinc site [14]. As a result the unit cell parameters do not vary significantly with increase in doping concentration. The same is observed in Fig. 2 for the ones (cobalt concentration ≤ 0.05 M) having lower local strain. From Fig. 2, it is also observed that the lattice constant of doped nanoparticles does not vary significantly where the local strain values are lower. However, lattice constant suffers a sudden change when cobalt concentration is greater than 0.05 M, reason for this sudden change in lattice constant can again be attributed to the elevated local strain induced by large amount of cobalt doping.

The particle size, shape and orientation of the cobalt-doped Zn_{0.9}Cd_{0.1}S nanoparticles were also determined by transmission electron microscopy. Electron diffraction pattern at different regions on the TEM grid for each sample were taken. We did not find any other diffraction rings that cannot be indexed by sphalerite structure. Figure 3a and c shows the TEM image for the nanoparticles with cobalt concentrations of 0.05 and 0.18 M,

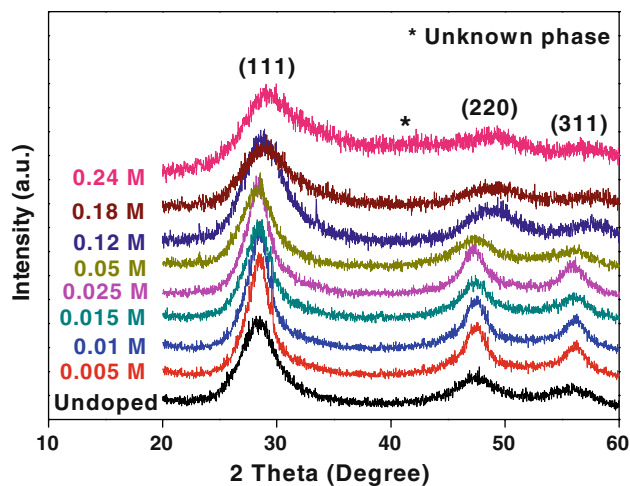


Fig. 1 X-ray diffraction patterns of Zn_{0.9}Cd_{0.1}S: yCo (undoped, 0.005, 0.01, 0.015, 0.025, 0.05, 0.12, 0.18 and 0.24 M) nanoparticles

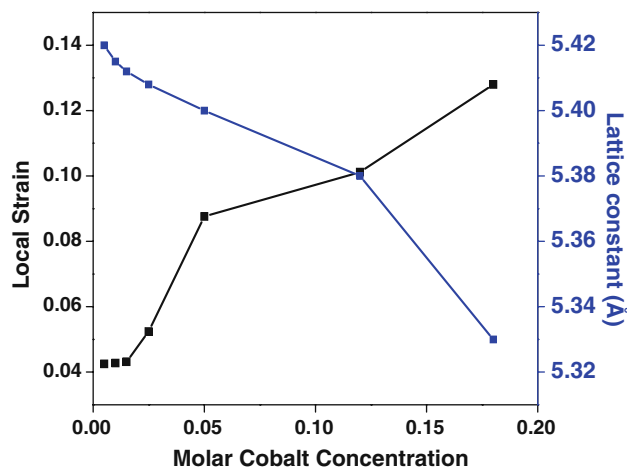


Fig. 2 Variation in local strain and lattice constant with cobalt concentration in Zn_{0.9}Cd_{0.1}S: yCo (0.005, 0.01, 0.015, 0.025, 0.05, 0.12 and 0.18 M) nanoparticles

respectively. TEM images shows nearly spherical particles and having average particle size of ~3.5 nm for both the samples. Figure 3b and d shows the selected area electron

Table 1 Cobalt molar concentrations in starting solution, y analysed from EPMA, average particle size, local strain, lattice constant as obtained by XRD, and energy band gap as determined by UV–Vis measurements

Molar Cobalt in starting solution	y of Zn _{1-x} Cd _x S: yCo	d _{XRD} (nm)	Local strain	Lattice constant (Å)	Band gap (eV)
0.005	0.0045	3.8	0.0425	5.391	3.81
0.010	0.0077	3.8	0.0428	5.387	3.76
0.015	0.0091	3.6	0.0432	5.384	3.71
0.025	0.0122	3.5	0.0524	5.376	3.66
0.050	0.0202	3.1	0.0876	5.364	3.60
0.12	0.04	2.2	0.1012	5.38	3.29
0.18	0.078	2.0	0.128	5.33	3.09
0.24	Unknown phase appeared				

diffraction pattern characteristic of a sphalerite phase for the nanoparticles with cobalt concentration of 0.05 and 0.18 M, respectively. In Fig. 3b, the first ring indicates a periodical structure with length of 3.1 Å, which is coincident with the standard sphalerite $\text{Zn}_{0.9}\text{Cd}_{0.1}\text{S}$ interplanar distance of 3.126 Å in the (111) direction, which is essentially the same as that obtained by Vegard's law [34] within experimental uncertainties, establishing the internal consistency between independent measurements.

TEM observation reveals the particle size of ~ 3.5 nm for both the samples considered. XRD measurements reveal the particle size of ~ 3.5 nm for the low cobalt concentration (≤ 0.05 M) and are in agreement with the result obtained from the TEM. For high cobalt concentration (>0.05 M) there exist a large discrepancy in particle sizes obtained via XRD and TEM. Difference in the particle sizes calculated from XRD and observed from TEM can be attributed to the distorted lattice structure, where both anion (S^{2-}) and cation (Zn^{2+}) deviate from standard tetrahedral coordination. Ren et al. [15] have also reported

the similar discrepancy in the particle sizes on increasing the cobalt doping in ZnS nanoparticles.

The dependence of Absorption coefficient (α) on energy ($h\nu$) near the band edge for cobalt-doped alloyed nanoparticles is shown in Fig. 4. It can be seen that there is a difference in slope between low (cobalt concentration ≤ 0.05 M) and high (cobalt concentration > 0.05 M) cobalt concentrations in the wavelength range of 320–430 nm. In a crystalline or polycrystalline material, direct or indirect optical transitions are possible depending on the band structure of the material. It was suggested that the extended absorption-edge spectrum of a normal direct band gap semiconductor, such as TiO_2 , usually indicates the possibility of indirect transitions [35].

The usual method of determining band gap is to plot a graph between $\alpha h\nu$ and $h\nu$ and look for that value of n which gives best linear graph in the band edge region [36]. We plotted $(\alpha h\nu)^{1/n}$ versus $h\nu$ for $\text{Zn}_{0.9}\text{Cd}_{0.1}\text{S}:\text{yCo}$ nanoparticles for each of the cobalt concentration, and the best fit were obtained for $n = 1/2$ for the samples for low cobalt

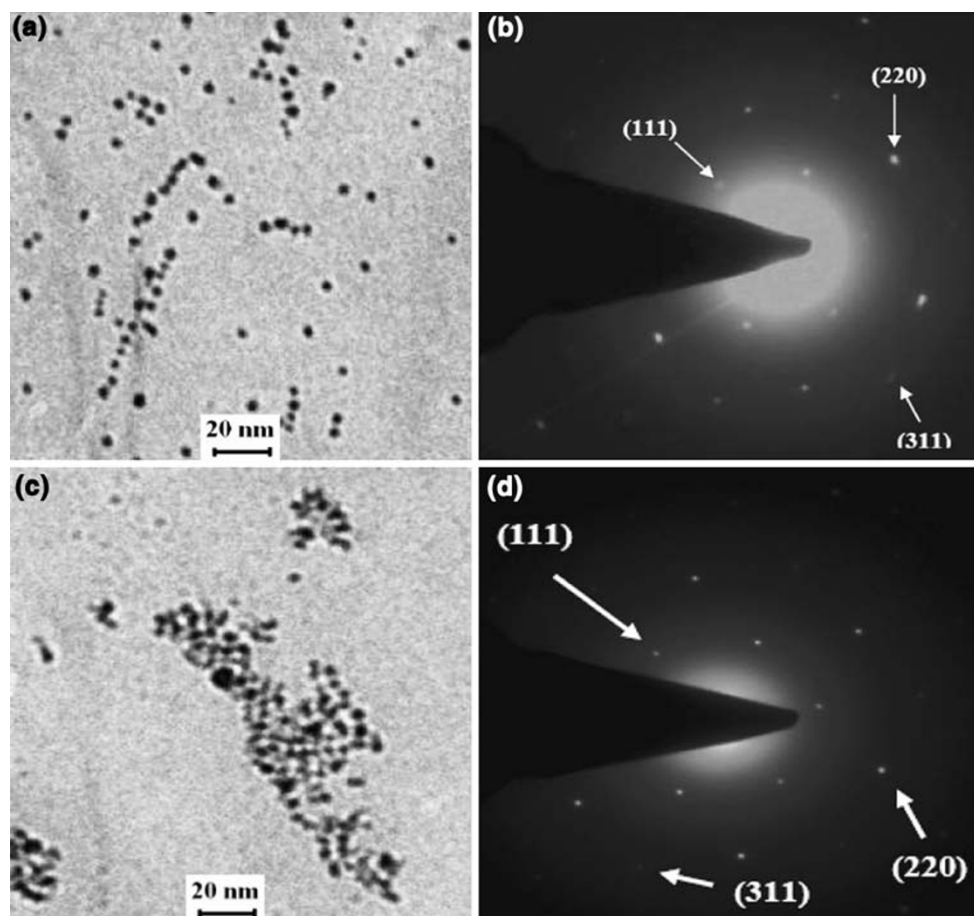


Fig. 3 (a, c) TEM images of $\text{Zn}_{0.9}\text{Cd}_{0.1}\text{S}:\text{0.0202Co}$ and $\text{Zn}_{0.9}\text{Cd}_{0.1}\text{S}:\text{0.078Co}$ nanoparticles. (b, d) Selected area electron diffraction patterns of $\text{Zn}_{0.9}\text{Cd}_{0.1}\text{S}:\text{0.0202Co}$ and $\text{Zn}_{0.9}\text{Cd}_{0.1}\text{S}:\text{0.078Co}$ nanoparticles

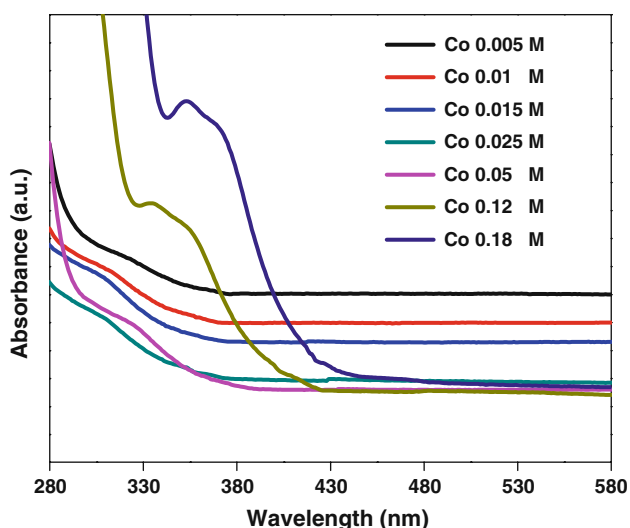


Fig. 4 Absorption spectra of $\text{Zn}_{0.9}\text{Cd}_{0.1}\text{S}:\text{yCo}$ (0.005, 0.01, 0.015, 0.025, 0.05, 0.12 and 0.18 M) nanoparticles

concentration (≤ 0.05 M) indicating a direct transition. For the high cobalt concentration (> 0.05 M) the best fit was obtained for $n = 2$, giving an evidence of an indirect transition. The appearance of change in gradients in the absorbance spectra at higher cobalt concentration might be caused by the deviation of lattice structure from undoped sample.

In the case of alloyed nanoparticles, the band gap energies are determined by their size and composition i.e., quantum confinement effect [37] and alloying effect [34]. In bulk CdS–ZnS alloyed crystals their composition (x)-dependent band gap energies ($E_g(x)$) can be expressed by Vegard's Law [34]:

$$E_g(x) = E_g(\text{ZnS}) + [E_g(\text{CdS}) - E_g(\text{ZnS}) - b]x + bx^2 \quad (1)$$

where $E_g(\text{ZnS})$ and $E_g(\text{CdS})$ are the band gap energies for bulk ZnS and CdS, respectively, and b is the bowing parameter and has the value 0.61 [34, 38]. For $\text{Zn}_{1-x}\text{Cd}_x\text{S}$ nanoparticles with particle size of 3.5 nm, Cd composition of 0.05 M, the band gap energy for the host system i.e., $\text{Zn}_{0.9}\text{Cd}_{0.1}\text{S}$ can be calculated using Eq. (1). Brus showed that semiconductor nanoparticles with a particle radius significantly smaller than the exciton Bohr radius exhibit strong size-dependent optical properties due to the strong quantum confinement effect (QCE) [37]:

$$E_g = E_g^0 + \frac{h^2}{8\mu R^2} - \frac{1.8e^2}{4\pi\epsilon R} \quad (2)$$

where E_g^0 is the energy band gap for the bulk material, R is the radius of the nanoparticle calculated from XRD data, $1/\mu = 1/m_e + 1/m_h$ (m_e and m_h being the electron and hole effective masses, respectively), ϵ is the dielectric constant

and e is the electronic charge. Here the electron effective mass (m_e), hole effective mass (m_h) and dielectric constant (ϵ) for ZnS are $0.25 m_0$, $0.51 m_0$ and $5.2 \epsilon_0$, respectively [39]. Corresponding values for CdS are $0.19 m_0$, $0.8 m_0$ and $5.7 \epsilon_0$ [39]. By substituting these values in Eq. 2, size-dependent band gap energy value of 4.005 and 2.97 eV for ZnS and CdS, respectively, are obtained. Therefore, instead of using 3.6 eV for ZnS and 2.38 eV for CdS [40], 4.005 eV for ZnS nanoparticles and 2.97 eV for CdS nanoparticles are plugged into Eq. 1 and the resulting composition (x)-dependent band gap energy of 3.84 eV is obtained for undoped $\text{Zn}_{0.9}\text{Cd}_{0.1}\text{S}$ alloyed nanoparticles. Figure 5a shows the direct band gap of the $\text{Zn}_{0.9}\text{Cd}_{0.1}\text{S}:\text{yCo}$ alloyed nanoparticles for the low cobalt concentration (≤ 0.05 M). The energy band gap for undoped sample ($E_g = 3.87$ eV) obtained from UV–Vis measurements was in agreement with the composition-dependent quantum confined energy band gap ($E_g = 3.84$ eV). The direct energy band gap, 3.81, 3.76, 3.71, 3.66 and 3.60 eV, corresponding to cobalt concentrations of 0.005, 0.01, 0.015, 0.025 and 0.05 M, respectively are obtained. Indirect energy band gap for the high cobalt concentration (> 0.05 M) is shown in Fig. 5b. Energy band gap of 3.29 and 3.09 eV is obtained for the cobalt concentrations of 0.12, and 0.18 M. It can also be observed that there is a decrease in energy band gap values with increase in cobalt concentration. This red shift of the energy band gap with increasing cobalt concentration is interpreted as mainly due to the sp–d exchange interactions between the band electrons and the localized d electrons of the Co^{2+} ions substituting host ions and is consistent with the reported results [41], giving an additional evidence of cobalt substitution.

Figure 6a and b shows the field-dependent magnetization (M – H) curves of nanoparticles with cobalt concentrations of 0.05 and 0.18 M, respectively, at 5, 50, 100 and 300 K temperatures. The curves show no hysteresis and no remanence, indicating no ferromagnetism for both the samples. Kang et al. [42] have reported ferromagnetic character of cobalt-doped ZnS powder presenting identical X-ray diffraction patterns but prepared using high temperature route. However, Ren et al. [15] have reported a paramagnetic behaviour of cobalt-doped ZnS nanoparticles. It can be observed from Fig. 6 that the magnetic moment (M) increases with increase in external field (H), typical feature of paramagnetic behaviour. According to Langevin model of paramagnetism [43], it is a system where localized non-interacting electronic magnetic moments on the atomic sites are randomly oriented as a result of their thermal energy. From the M – H measurements, it is clear that even at 5 K the sample shows hysteresis curve with almost zero coercivity which rules out the possibility of ferromagnetic ordering. Since thermal

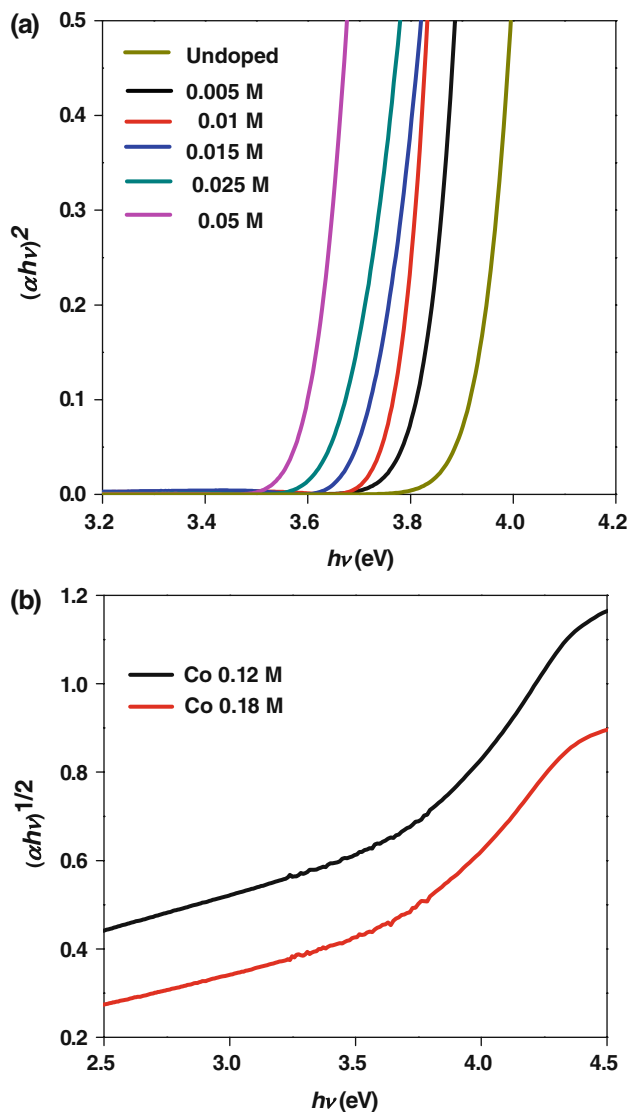


Fig. 5 **a** $(\alpha hv)^2$ versus $h\nu$ plots of $Zn_{0.9}Cd_{0.1}S:yCo$ nanoparticles for undoped, 0.005, 0.01, 0.015, 0.025 and 0.05 M. **b** $(\alpha hv)^{1/2}$ versus $h\nu$ $Zn_{0.9}Cd_{0.1}S:yCo$ nanoparticles for 0.12 and 0.18 M

agitations are little at 5 K, the Co^{2+} ions can get coupled antiferromagnetically and thus could give rise to antiferromagnetic coupling. For the sake of comparison $M-H$ measurements of undoped sample were also taken at 5 and 300 K and are shown in Fig. 6c. The pure $Zn_{0.9}Cd_{0.1}S$ sample exhibited, as expected, a diamagnetic behaviour. No difference is observed between the magnetizations measured at 5 and 300 K for the undoped sample.

Temperature dependence of magnetization of nanoparticles with cobalt concentrations of 0.05 and 0.18 M in a field of 500 Oe are shown in Fig. 7a and b, respectively. It can be observed from Fig. 7 that both the samples show a very small magnetic moment for the temperature range from 300 to 70 K but as the temperature falls below 70 K

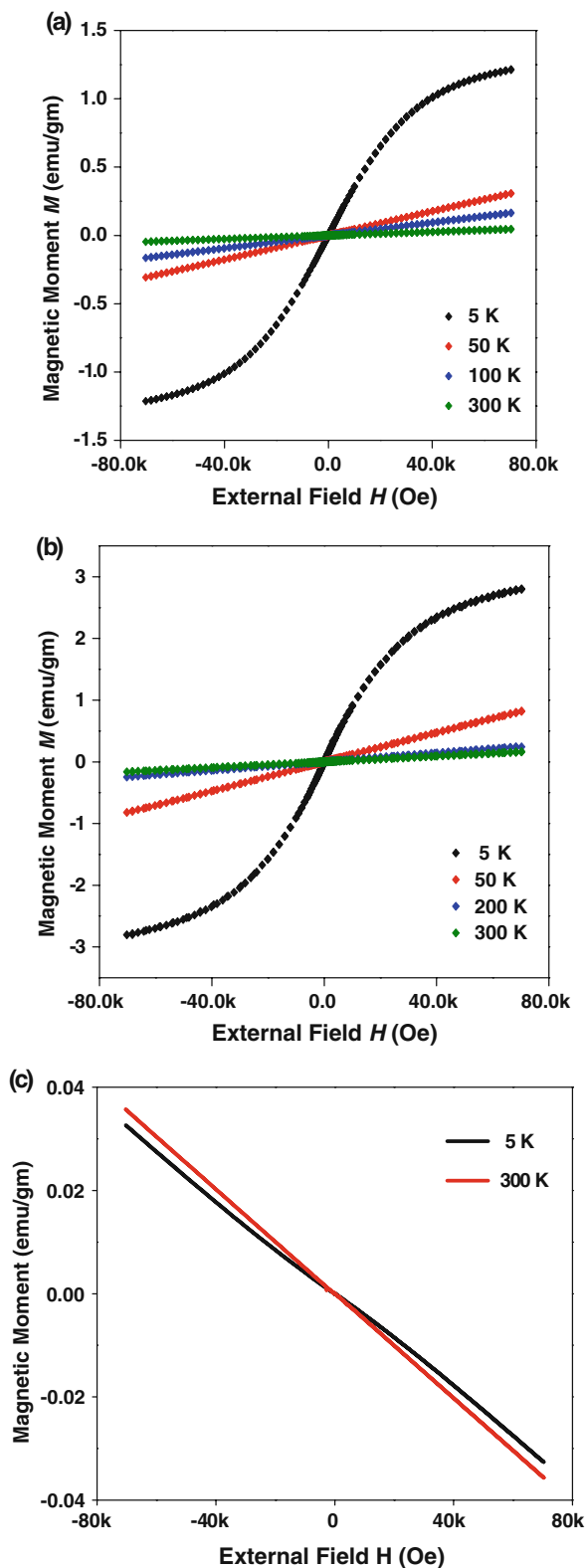


Fig. 6 Magnetization versus applied magnetic field measured at 5, 50, 100 and 300 K. **a** 0.05 M cobalt concentration, **b** 0.18 M cobalt concentration, **c** Magnetization versus applied magnetic field for undoped sample at 5 and 300 K

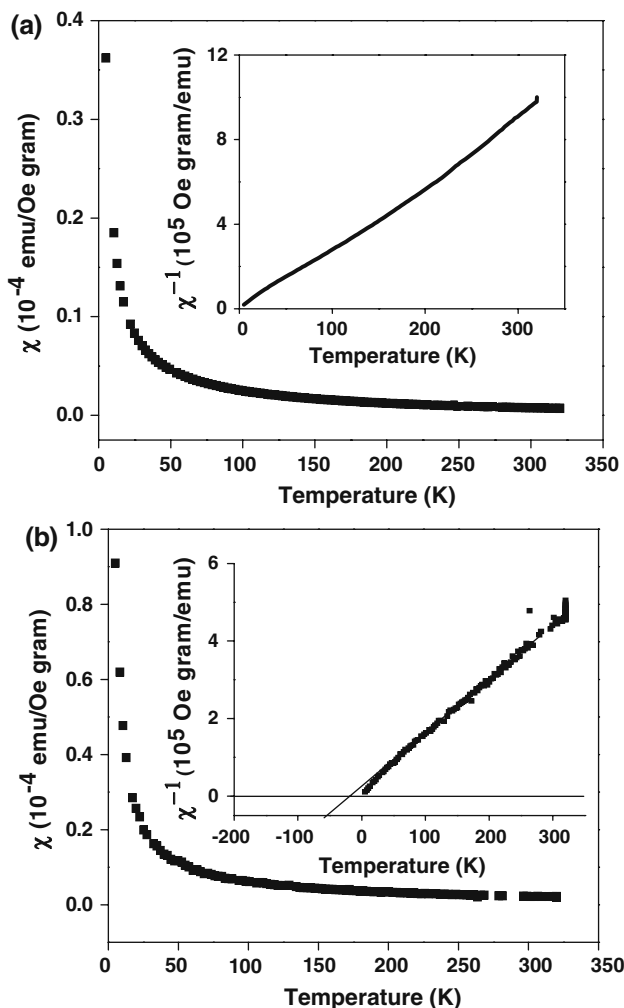


Fig. 7 Temperature-dependent magnetic mass susceptibility measured under a magnetic field of 500 Oe. *Inset:* inverse susceptibility as a function of temperature: **a** 0.05 M cobalt concentration, **b** 0.18 M cobalt concentration

the paramagnetic properties dominates and the magnetization increases. Inset in Fig. 7a and b displayed the inverse susceptibility (χ^{-1}) as a function of temperature with cobalt concentrations of 0.05 and 0.18 M, respectively. The result is consistent with the Curie–Weiss equation [43]:

$$\chi = C / (T + \theta) \tag{3}$$

where χ is the magnetic susceptibility, C is the paramagnetic Curie constant and θ is the Curie–Weiss temperature. It can be observed from the inset of Fig. 7a that the curve passes through the origin indicating nanoparticles (with 0.05 M cobalt concentration) are paramagnetic in nature, giving no evidence for antiferromagnetic coupling. However, the plot of χ^{-1} versus T (with cobalt concentration of 0.18 M) in the inset of Fig. 7b does not pass through the origin. Extrapolation of the linear part of this curve gives

an intercepts on the negative temperature axis around -75 K (Curie–Weiss temperature, θ), indicating the antiferromagnetic exchange between cobalt magnetic moments [15]. The reason for this can be attributed to the increased number of Co^{2+} ions in the $\text{Zn}_{0.9}\text{Cd}_{0.1}\text{S}$ lattice which gave fairly possible opportunity to interact. This has also been verified by plotting the curve between χT and T , where T is the temperature and is shown in Fig. 8. It can be observed that χT increases with increasing temperature, a typical signature of antiferromagnetic behaviour [44].

Bouloudein et al. [44] have considered in their study that the ferromagnetism in DMS is originated from the exchange interaction between free delocalized carriers and the localized d spins of the cobalt ions. Presence of free carriers is therefore necessary for the appearance of ferromagnetism. Free carriers can be induced either by doping or by defects or by cobalt ions in another oxidation state like Co^{3+} . Above explanation suggests that our samples have limited number of impurities or defects, which may explain the absence of free carriers and consequently the ferromagnetism.

The most direct and immediate evidence for the alloying process for undoped $\text{Zn}_{0.9}\text{Cd}_{0.1}\text{S}$ nanoparticles can be probed from the XRD peak position and the energy band gap obtained from UV–Vis measurement, found in consistent with the Vegard’s law, indicating the homogeneous distribution of ZnS and CdS in the alloyed nanocrystals. We also believe that there is no signature of CoS or other impurity phases in our samples. XRD does not show any detectable signal of Co or CoS, which means that the content of CoS or Co in the samples is at most less than 5% (5% is the detection limit of XRD). TEM diffraction pattern also supports our argument as we did not find any other diffraction rings in our TEM diffraction pattern that

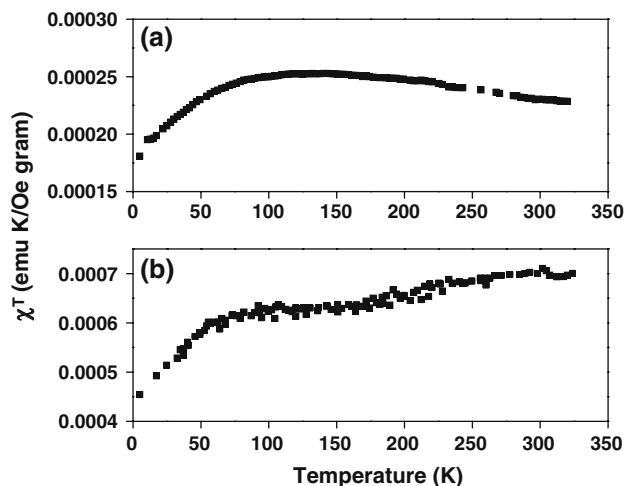


Fig. 8 Variation of χT with temperature. **a** 0.05 M cobalt concentration, **b** 0.18 M cobalt concentration

cannot be indexed by sphalerite structure. Also, if there is even a trace amount of ferromagnetic Co in the precipitates, the sample will exhibit ferromagnetism. Nanoparticles with low cobalt concentration are paramagnetic at 5 K, while the nanoparticles with high cobalt concentrations give rise to antiferromagnetism coupling, but the ferromagnetism did not appear at all. This eliminates the possibility of ferromagnetic cobalt existing in the samples. In this study, we found that the physical properties of $Zn_{0.9}Cd_{0.1}S: \gamma Co$ nanoparticles produced at different cobalt concentration are obviously different. Low cobalt concentration samples (≤ 0.05 M) have less distortion of the tetrahedral coordination of Co^{2+} ions and direct band gap absorption, while high cobalt concentration samples (> 0.05 M) have more distortion of the tetrahedral coordination of Co^{2+} and indirect band gap absorption.

Conclusions

In summary, we have presented the synthesis of $Zn_{0.9}Cd_{0.1}S: \gamma Co$ alloyed nanoparticles from a solution-based synthetic route. Structural, optical and magnetic characterizations confirm that the cobalt doping is substitutional for zinc cations in the host lattice. The doping concentration in the alloyed nanoparticles can be divided into two distinct regions, low (≤ 0.05 M) and high (> 0.05 M) cobalt concentration corresponding to the Co^{2+} molar percentage in the starting solution. Accordingly the structural, optical and magnetic properties were found distinctively different. A red shift in the energy band gap is found with increasing cobalt concentration. Cobalt-doped $Zn_{0.9}Cd_{0.1}S$ nanoparticles are found to have paramagnetic nature for the nanoparticles with cobalt concentration of 0.05 M (low cobalt concentration). Nanoparticles with cobalt concentration of 0.18 M (high cobalt concentration) found to have antiferromagnetic coupling with negative Curie–Weiss temperature of -75 K. These findings have important implications for the optical and the magnetic materials, where the physical properties get significantly affected on increasing the doping.

Acknowledgements One of the authors, Amit Kumar Chawla, thanks CSIR, New Delhi for the award of research associate. The financial support by DST [Grant No. SR/S5NM-32/2005] New Delhi is gratefully acknowledged.

References

1. S.J. Pearton, D.P. Norton, K. Ip, Y.W. Heo, T. Steiner, *J. Vac. Sci. Technol.* **22**, 932 (2004)
2. A.H. Macdonald, P. Shiffer, N. Samarth, *Nat. Mater.* **4**, 195 (2005)
3. H. Ohno, *Science* **281**, 951 (1998)
4. C.Q. Zhu, P. Wang, X. Wang, Y. Li, *Nanoscale Res. Lett.* **3**, 213 (2008)
5. W. Luan, H. Yang, N. Fan, S.T. Tu, *Nanoscale Res. Lett.* **3**, 134 (2008)
6. D. Jiang, L. Cao, G. Su, W. Liu, H. Qu, Y. Sun, B. Dong, *Mater. Chem. Phys.* **44**, 2792 (2009)
7. L. Wang, H. Wei, Y. Fan, X. Liu, J. Zhan, *Nanoscale Res. Lett.* **4**, 558 (2009)
8. M. Protière, P. Reiss, *Nanoscale Res. Lett.* **1**, 62 (2006)
9. D. Jiang, L. Cao, W. Liu, G.S.H. Qu, Y. Sun, B. Dong, *Nanoscale Res. Lett.* **4**, 78 (2009)
10. X. Zhong, Y. Feng, *Res. Chem. Intermed.* **34**, 287 (2008)
11. R. Sethi, L. Kumar, A.C. Pandey, *J. Nanosci. Nanotechnol.* **9**, 1 (2009)
12. R. Sanz, J. Jensen, G.G. Díaz, O. Martínez, M. Vázquez, M.H. Vélez, *Nanoscale Res. Lett.* **4**, 878 (2009)
13. H. Shi, Y. Duan, *Nanoscale Res. Lett.* **4**, 480 (2009)
14. P. Singh, R.N.G. Deepak, A.K. Pandey, D. Kaur, *J. Phys. Condens. Matter.* **20**, 315005 (2008)
15. G. Ren, Z. Lin, C. Wang, W. Liu, J. Zhang, F. Huang, J. Liang, *Nanotechnology* **18**, 035705 (2007)
16. C. Yan, J. Liu, F. Liu, J. Wu, K. Gao, D. Xue, *Nanoscale Res. Lett.* **3**, 473 (2008)
17. H. Peng, B. Liuyang, Y. Lingjie, L. Jinlin, Y. Fangli, C. Yunfa, *Nanoscale Res. Lett.* **4**, 1047 (2009)
18. S.K. Mehta, S. Kumar, S. Chaudhary, K.K. Bhasin, M. Gradzielski, *Nanoscale Res. Lett.* **4**, 17 (2009)
19. J. Antony, S. Pendyala, A. Sharma, X.B. Chen, J. Morrison, L. Bergman, Y. Qiang, *J. Appl. Phys.* **97**, 10D307 (2005)
20. P.V. Radovanovic, D.R. Gamelin, *J. Am. Chem. Soc.* **123**, 12207 (2001)
21. F.V. Mikulec, M. Kuno, M. Bennati, D.A. Hall, R.G. Griffin, M.G. Bawendi, *J. Am. Chem. Soc.* **122**, 2532 (2000)
22. Y.M. Sung, Y.J. Lee, K.S. Park, *J. Am. Chem. Soc.* **128**, 9002 (2006)
23. H. Lee, H. Yang, P.H. Holloway, *J. Lumin.* **126**, 314 (2007)
24. S.A. Santangelo, E.A. Hinds, V.A. Vlaskin, P.I. Archer, D.R. Gamelin, *J. Am. Chem. Soc.* **129**, 3973 (2007)
25. R.E. Bailey, S.M. Nie, *J. Am. Chem. Soc.* **125**, 7100 (2003)
26. X.H. Zhong, Y.Y. Feng, W. Knoll, M.Y. Han, *J. Am. Chem. Soc.* **125**, 13559 (2003)
27. R.N. Bhargava, D. Gallagher, X. Hong, A. Nurmikko, *Phys. Rev. Lett.* **72**, 416 (1994)
28. M. Zielinski, C. Rigaux, A. Lemaitrie, A. Mycielskin, *Phys. Rev. B* **53**, 674 (1996)
29. M.J. Seong, H. Alawadhi, I. Miotkowski, A.K. Ramdas, *Phys. Rev. B* **63**, 125208 (2001)
30. S.W. Lu, B.I. Lee, Z.L. Wang, W. Tong, B.A. Wagner, W. Park, C.J. Summners, *J. Lumin.* **92**, 73 (2001)
31. S. Singhal, A.K. Chawla, H.O. Gupta, R. Chandra, *J. Nanopart. Res.* (2009). doi:10.1007/s11051-009-9687-x
32. B.D. Cullity, S.R. Stock, *Elements of X-Ray Diffraction*, 3rd edn. (Prentice Hall, Upper Saddle River, 2001), p. 170
33. D. Son, D.R. Jung, J. Kim, T. Moon, C. Kim, B. Park, *Appl. Phys. Lett.* **90**, 101910 (2007)
34. J. Singh, *Optoelectronics an introduction to materials and devices* (Macgraw Hill, New Delhi, 1996)
35. R. Zallen, M.P. Moret, *Solid State Commun.* **137**, 154 (2006)
36. J. Tauc (ed.), *Amorphous and Liquid Semiconductor* (Plenum Press, New York, 1974), p. 159
37. L.E. Brus, *J. Chem. Phys.* **80**, 4403 (1984)
38. S.M. Sze, *Physics of Semiconductor Devices* (Wiley, New York, 1969)
39. H. Ohde, M. Ohde, F. Bailey, H. Kim, C.M. Wai, *Nano Lett.* **2**, 721 (2002)

40. A. Goudarzi, G.M. Aval, R. Sahrai, H. Ahmadpoor, *Thin Solid Films* **516**, 4953 (2008)
41. N. Kumbhoikar, V.V. Nikesh, A. Kshirsagar, S. Mahamuni, *J. Appl. Phys.* **88**, 6260 (2000)
42. T. Kang, J. Sung, W. Shim, H. Moon, J. Cho, Y. Jo, W. Lee, B. Kim, *J. Phys. Chem. C* **113**, 5352 (2009)
43. B.D. Cullity, C.D. Graham, *Introduction to Magnetic Materials* (Addison-Wesley, Reading, 1972)
44. M. Bouloudenine, N. Viart, S. Colis, J. Kortus, A. Dinia, *Appl. Phys. Lett.* **87**, 052501 (2005)